

## EFFECT OF POWDER CHEMICAL COMPOSITION ON MICROSTRUCTURES AND MECHANICAL PROPERTIES OF L-PBF PROCESSED 17-4 PH STAINLESS STEEL IN THE AS-BUILT AND HARDENED-H900 CONDITIONS

S. Vunnam\*, S. Dobson\*, A. Saboo†, D. Frankel†, C. Sudbrack†, and T. L. Starr \*

\* J. B. Speed School of Engineering, University of Louisville, Louisville, KY, 40292, USA

†QuesTek Innovations LLC, 1820 Ridge Avenue, Evanston, IL USA 60201, USA

### Abstract

Post-build heat treatments such as solutionizing and precipitation hardening are recommended for selective laser melting (SLM) processed components to achieve a homogeneous microstructure. In this study, the effect of powder elemental composition on microstructures and mechanical properties of SLM processed 17-4 PH was studied in the as-built and precipitation hardened (H900) condition without prior solutionizing. Microstructural characterization demonstrated that H900 increased martensite phase composition for samples from powder with low chromium to nickel equivalent ( $\text{Cr}_{\text{eq}}/\text{Ni}_{\text{eq}}$ ) value, whereas no significant difference was observed for the samples from powders with high  $\text{Cr}_{\text{eq}}/\text{Ni}_{\text{eq}}$  value. None of the specimens exhibited austenite reversion and strain hardening behavior in the as-built and H900 conditions. Low  $\text{Cr}_{\text{eq}}/\text{Ni}_{\text{eq}}$  specimen exhibited higher yield and tensile strengths, and microhardness from H900, which are comparable to H900 wrought sample. However, no significant improvement in total elongation was observed other than uniform elongation for low  $\text{Cr}_{\text{eq}}/\text{Ni}_{\text{eq}}$  specimen.

*Keywords:* 17-4 PH stainless steel, Selective laser melting, Electron backscatter diffraction (EBSD), Phase composition, Mechanical Properties, H900 hardening

### Introduction

Laser powder bed fusion (L-PBF) processing of precipitation hardenable (PH) martensitic stainless steels, specifically 17-4 PH, are of great interest because of their unique combination of high strength and corrosion resistance. The microstructure and mechanical properties of L-PBF processed 17-4 PH stainless steel alloy parts are highly dependent on the powder chemical composition and the post-build heat treatments. Recent studies focused on improving yield strength, hardness and fatigue behavior by optimizing processing conditions and heat treatments [1-7]. State of the art literature on L-PBF processed 17-4 PH reveals a strong dependence of material microstructure and phase constitution on process parameters, particularly the presence of a significant fraction of retained austenite [1, 3, 4, 8] or retained δ ferrite [9] in the as-built condition. Extremely high temperature gradients induce nonhomogeneous grain size and residual stresses in L-PBF parts [10, 11]. Post-build heat treatments were recommended to relieve the stress and to obtain uniform grain size. Solutionizing is used for uniform distribution of the elements in the alloy, whereas precipitation hardening induces nanoscale Cu rich precipitates which play a key role in enhancing the mechanical strength and hardness. However, heat treatments are time consuming and expensive. Very limited research has been focused on microstructure and mechanical properties in the as-built condition as well as H900 condition without prior solutionizing. The effect of atomizing gas on microstructure and mechanical properties in the as-built and hardened condition was studied [12]. Hardening using H900 alone without solutionizing inhibited strengthening due to the large volume of retained austenite [13]. However, the alloy

powder chemical composition effect on microstructure and tensile properties was not explored in detail. The objective of the current study is to determine the effect of powder chemical composition on the microstructure and mechanical properties of L-PBF processed 17-4 PH in the as-built and H900 conditions. Previous work by the authors of this paper outlined the L-PBF processed 17-4 PH texture and phase composition sensitivity to powder chemical composition in the as-built condition [14]. Powder with lower  $\text{Cr}_{\text{eq}}/\text{Ni}_{\text{eq}}$  value produced a component with largely martensitic phase with some residual  $\delta$  ferrite and retained austenite. In this study, microstructure and mechanical properties of components from three different commercially available Ar-atomized 17-4 PH powders that conforms to the UNS S17400 specification range were explored in the as-built and H900 conditions and compared with wrought under identical conditions. In-depth microstructure characterization was carried out using optical microscopy (OM) and electron backscatter diffraction (EBSD) techniques. Microhardness and tensile properties were measured to validate the microstructural analysis.

## Experimental

In this study, 17-4 PH stainless steel test specimens were built using a commercial EOSINT M290 SLM machine. Three commercially available Ar-atomized powders (Powder A, Powder B and Powder C) with a different chemical composition that conforms to the UNS S17400 specification range were used for this study. The chemical composition of wrought 17-4 PH and the three powders and  $\text{Cr}_{\text{eq}}/\text{Ni}_{\text{eq}}$  values based on WRC-1992 equations were tabulated in Table 1 [15]. All the test specimens were fabricated with the optimized SLM parameters using a standard build strategy, which involves bidirectional beam scanning with a scan rotation angle of  $67^\circ$ , and all the parts exhibited a full density. Detailed powder properties and part densities were discussed elsewhere [16]. Processing parameters deployed in this study included laser power of 190 W, scanning speed of 750 mm/s, hatch distance of 0.100 mm, layer thickness of 0.040 mm and build plate temperature of 40 °C. As-received wrought material and the as-built SLM test specimens were subjected to H900 heat treatment at 482 °C for 1 hour then air cooled. For shorthand notation, “AB” and “H900” suffixes attached to the name of the powder for the as-built and H900 conditions, respectively.

As-received (annealed) wrought samples (Wrought-AR) and H900 wrought samples (Wrought-H900) were cut such that the section surface is normal to the rolling direction. Metallographic sample preparation was done using a specific metallographic sample preparation method that can be found elsewhere [14]. The freshly polished sample’s surface was etched by a Kalling’s no. 2 reagent for 1 to 2 minutes using an immersion method. The etched samples were rinsed in isopropyl alcohol immediately and air-dried. The etched samples were examined along the build direction using an Olympus BX53 optical microscope. Samples were further polished using GIGA 0900 vibratory polisher using colloidal silica suspension for EBSD. EBSD was carried out at 20 kV using an FEI Teneo field emission SEM equipped with an EDAX TEAM EBSD system. For EBSD analysis, the polished samples from sections parallel to build direction were tilted  $70^\circ$  to the electron beam and 12 mm working distance was maintained. The step size used for the EBSD analysis ranges from 0.3 to 1.5  $\mu\text{m}$ . The EBSD data acquired were processed using TSL OIM analysis software.

Tensile testing was performed in an Instron 50 kN test machine (Model: 5569A) using ASTM E8-16 standard tensile testing method. Tensile testing specimens were machined out using electrical discharge machining (EDM) from the bulk material primitives according to the dimensions specified by the ASTM E8 standard to mitigate the surface related artifacts of the SLM process. The hardness of the samples was evaluated by performing Vickers micro-hardness measurements on the polished sections using Shimadzu's HMV-G21. At least 10 measurements were taken diagonally from each sample using a load of 980.67 mN (100 gf) with a 10 s holding time.

**Table 1.** Chemical composition (wt.%) of the three Ar-atomized 17-4 PH stainless steel powders and as-received wrought

	Cr	Ni	Mo	Nb+Ta	C	N	Cu	Mn	Si	Fe	Cr <sub>eq</sub> /Ni <sub>eq</sub>
Powder A	16.12	4.15	-	0.2	0.02	0.007	3.21	-	0.79	Bal.	2.81
Powder B	16.7	4.29	0.05	0.27	0.01	0.031	4.49	0.2	0.36	Bal.	2.65
Powder C	15.6	4.7	-	0.22	0.01	0.036	3.61	0.5	0.38	Bal.	2.36
Wrought	15-17.5	3-5	0-0.5	0-0.45	0-0.07	-	0-5.0	0-1.0	0-1.0	Bal.	-

\*Provider datasheet

\* $Cr_{eq} = Cr + Mo + (0.7 \times Nb)$

\* $Ni_{eq} = Ni + (35 \times C) + (20 \times N) + (0.25 \times Cu)$

## Results and Discussion

### **Microstructure and Phase Composition**

Optical micrographs of etched samples in the as-built and H900 conditions along the build direction are shown in Fig. 1. Powder A and Powder B samples have columnar grains that are grown across several melt pool boundaries along the build direction. Small martensitic laths can be seen below the melt pool boundary for Powder A sample. There is no significant difference observed in the microstructures of Powder A, Powder B and Powder C samples after H900 heat treatment from optical micrographs. Powder A and Powder B samples exhibited a large δ-ferrite phase constituent after H900 heat treatment similar to the as-built samples. However, Powder C sample has a fine grain microstructure in the as-built as well as in heated conditions. In order to get a more detailed understanding of Powder C sample microstructure, further analysis was performed using EBSD and compared with the Wrought-H900 sample. In-depth microstructure and phase evolution analysis for all three SLM samples in the as-built condition can be found elsewhere [14]. EBSD orientation maps obtained from an area of 400 μm x 300 μm for Powder C-H900 and Wrought-H900 are shown in Fig.2(a,b). FCC-austenite grains can be clearly seen in

higher magnification orientation maps obtained from an area of  $99 \mu\text{m} \times 72 \mu\text{m}$  as shown in Fig. 2(c, d) (separated by a black line). EBSD phase analysis indicates that austenite volume fraction in Powder C-H900 and Wrought-H900 samples are 2.3 and 1.2%, respectively. Powder C-H900 sample exhibited inhomogeneous grain size distribution by having coarse columnar grains whereas, Wrought-H900 has more homogeneous grain size distribution. The average grain size for Powder C-H900 sample is  $9.5 \mu\text{m}$  including FCC and BCC grains by excluding low angle grain boundaries (LAGBS) for martensitic laths. The average martensitic block size for Powder C-H900 and Wrought-H900 samples are  $12.6$  and  $4.3 \mu\text{m}$ , respectively. Powder C-H900 sample has fine grain regions from transformed martensite whereas coarse columnar grains are from retained  $\delta$  ferrite [14]. Fig. 3 shows overlay of orientation and image quality (IQ) maps for same maps from Fig. 2(c, d). It can be seen the darker contrast within the grains in martensitic region due to the poor image quality from the distorted BCT crystal structure. EBSD grain boundary maps corresponding to orientation maps in Fig. 2(c, d) and 3 (a, b) are shown in Fig. 3(c, d). Grain boundaries are color-coded by green ( $2-17^\circ$ ), red ( $17-49^\circ$ ) and black ( $49-180^\circ$ ). LAGBs ( $2-17^\circ$ ) were observed in the fine grain region but not in the columnar grains for Powder C-H900 sample indicating that columnar grains are  $\delta$  ferrite grains and were not transformed to martensite upon cooling. The linear fraction of LAGBs for Powder-C sample is 48.1% and increased from 35% in the as-built condition [14]. The linear fraction of Wrought-H900 sample is 59.6% and these are uniformly distributed throughout the specimen. As shown in Fig. 4, frequency of martensitic boundaries observed above  $49^\circ$  and below  $17^\circ$ . Parent austenite grain boundaries and lath boundaries (specifically wrought sample) can be seen in Fig. 3(a, b) which arise from the IQ contrast. As shown in Fig. 3(c,d), grain boundaries that are drawn using misorientation angle  $17^\circ-49^\circ$  (red) are in good agreement with parent austenite grain boundaries seen in Fig. 3(a, b).

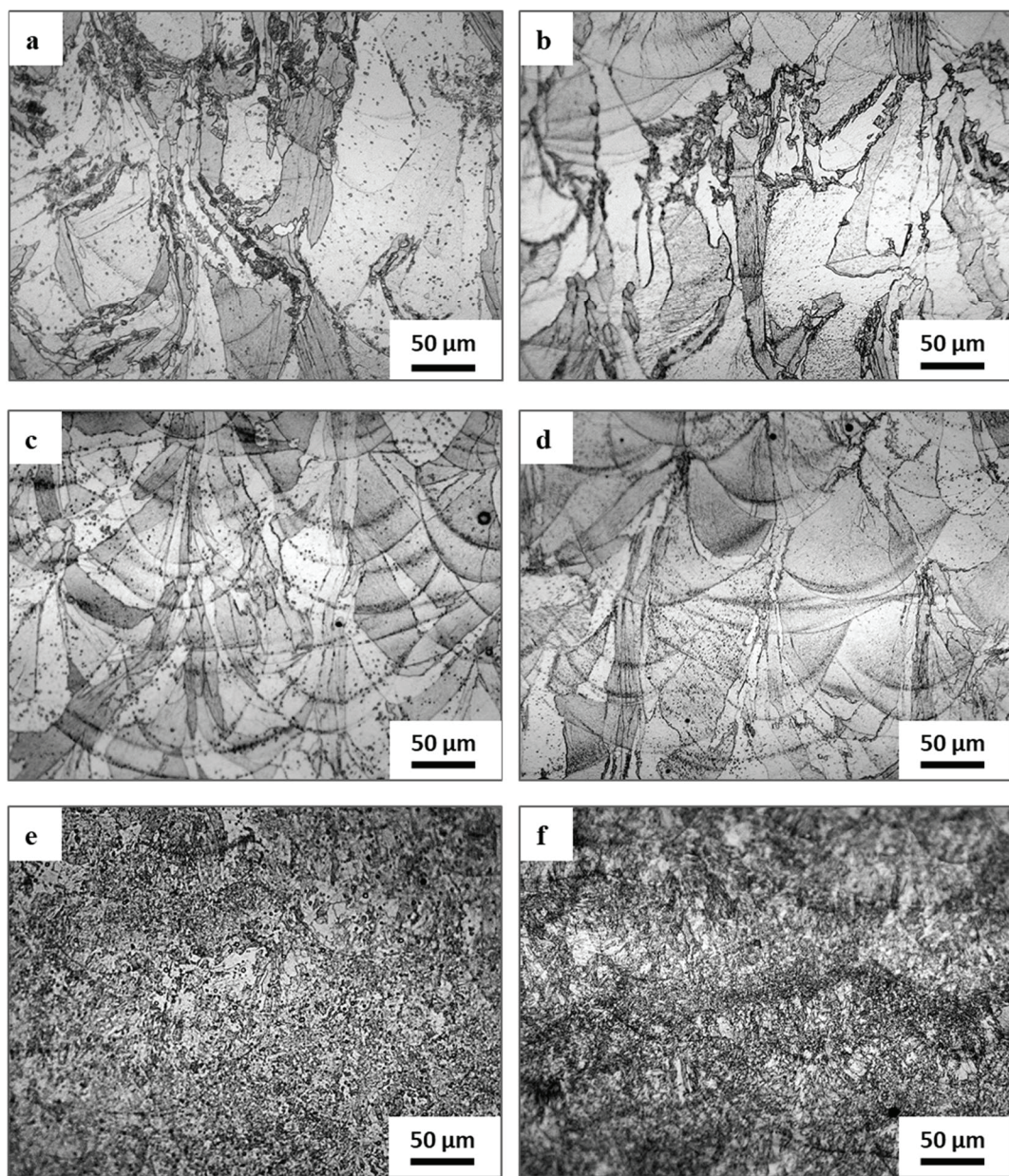


Fig. 1. Optical micrographs of etched 17-4 PH metallographic sections: As-built (a) Powder A, (c) Powder B and (e) Powder C; H900 (b) Powder A, (d) and Powder B (f) Powder C

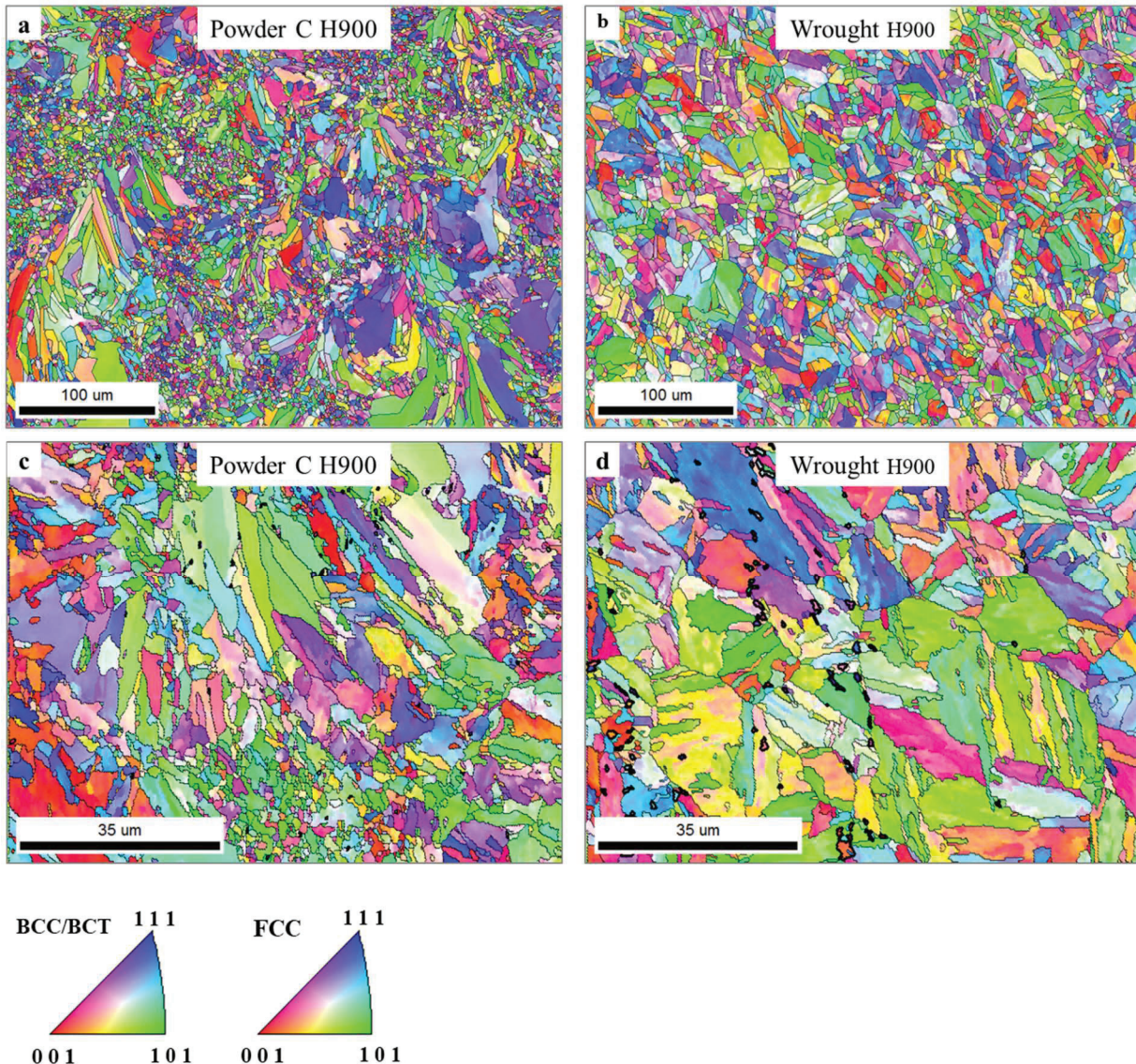


Fig. 2. EBSD orientation maps (a, c) Powder C H900, (b, d) Wrought H900

(100) pole figures corresponding to the EBSD orientation maps (Fig. 2(c, d)) are shown in Fig. 5. Both Powder C-H900 and Wrought-H900 samples have higher {100} texture strength compared to {110} and {111}. Weaker {100} texture strength for Powder C-H900 sample compared to Wrought-H900 sample could be due to the large grain growth rate, which led to parent austenite grain refinement which can be seen in Fig. 3(c). Stronger texture for wrought sample can be due to large plastic deformation and subsequent recrystallization from hot rolling as the sample surface is normal to the rolling direction [17].

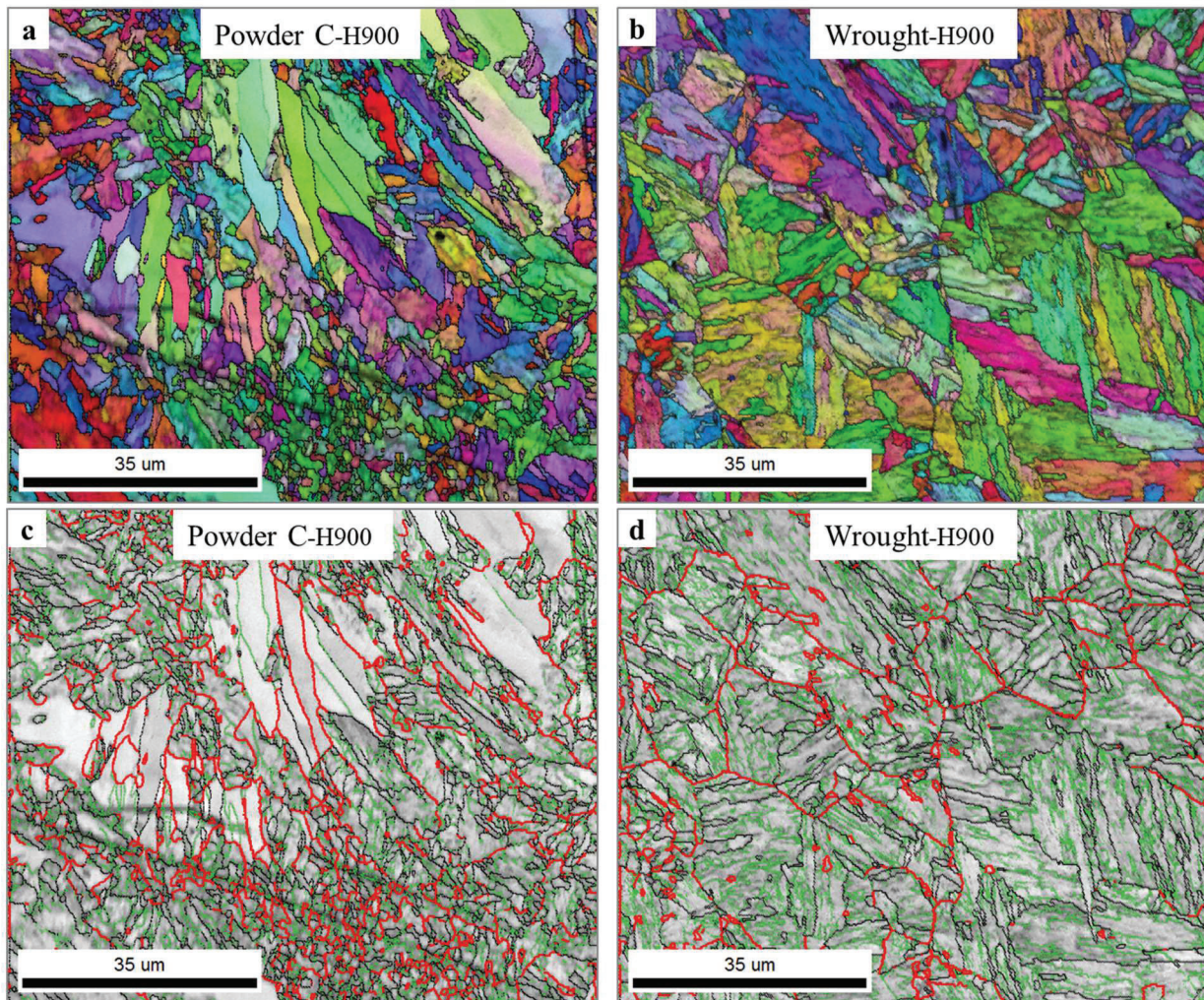


Fig. 3. EBSD IPF and IQ overlay maps (a, b), grain boundary misorientation maps:  $2^\circ$ – $17^\circ$ (green),  $17^\circ$ – $49^\circ$ (red), and  $49^\circ$ – $180^\circ$ (black)

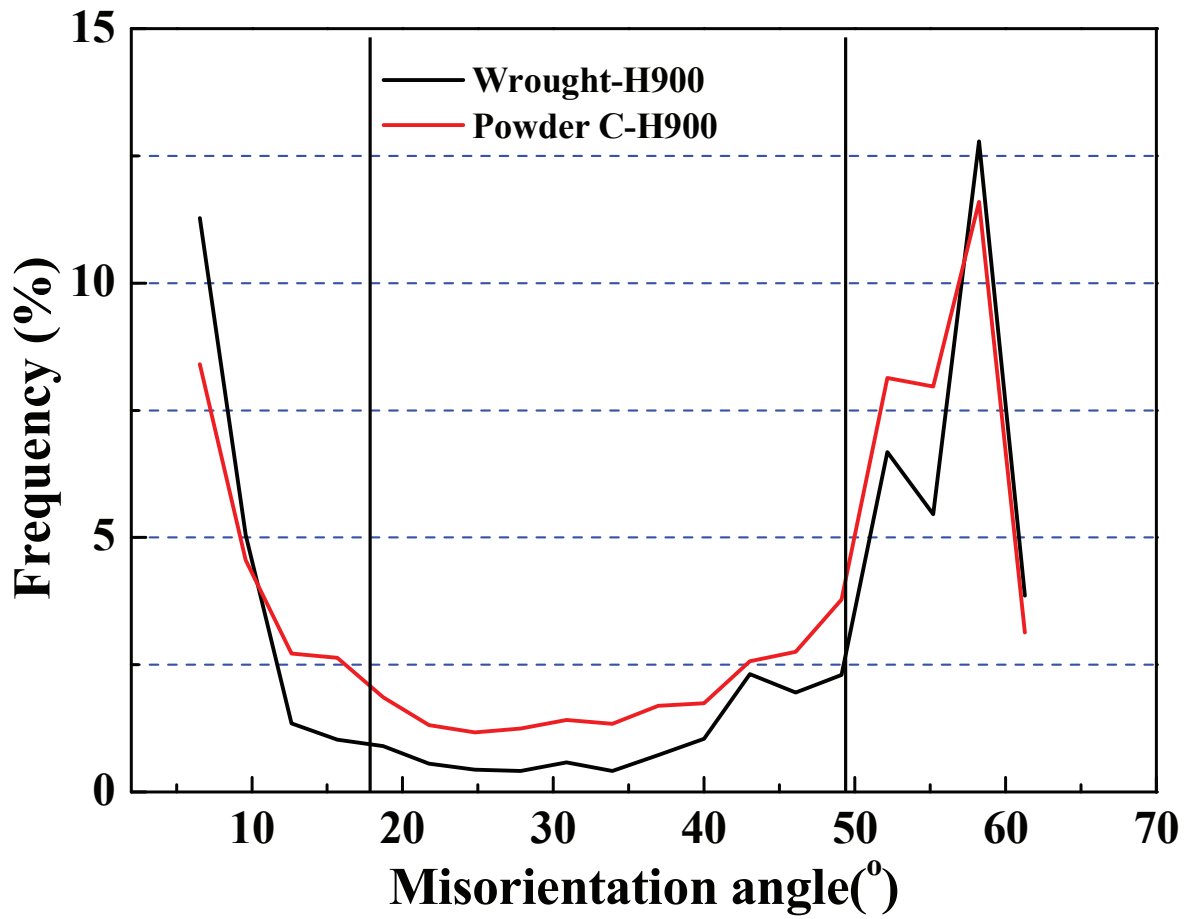


Fig. 4. The frequency distribution of parent austenite grain boundaries vs. misorientation angle

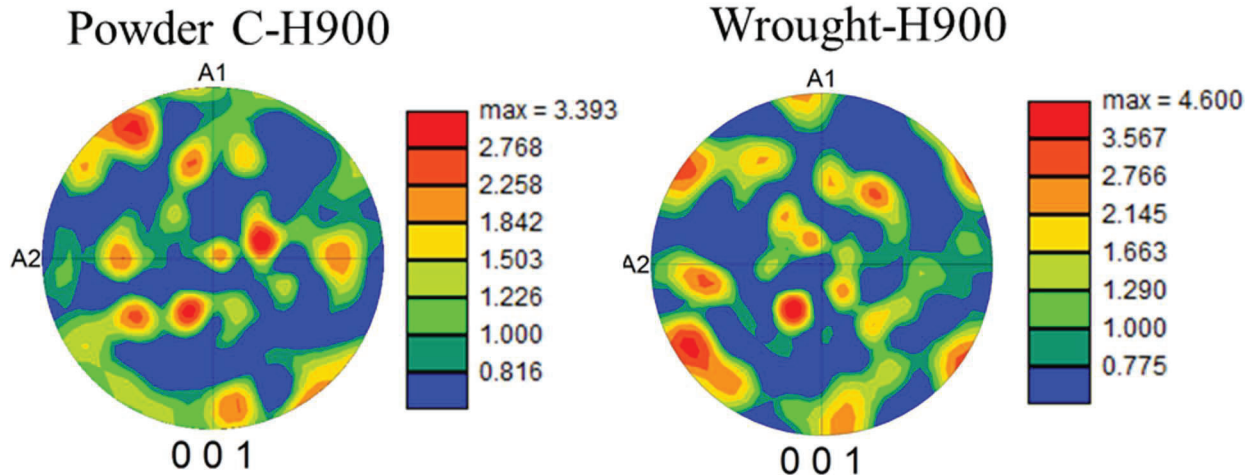
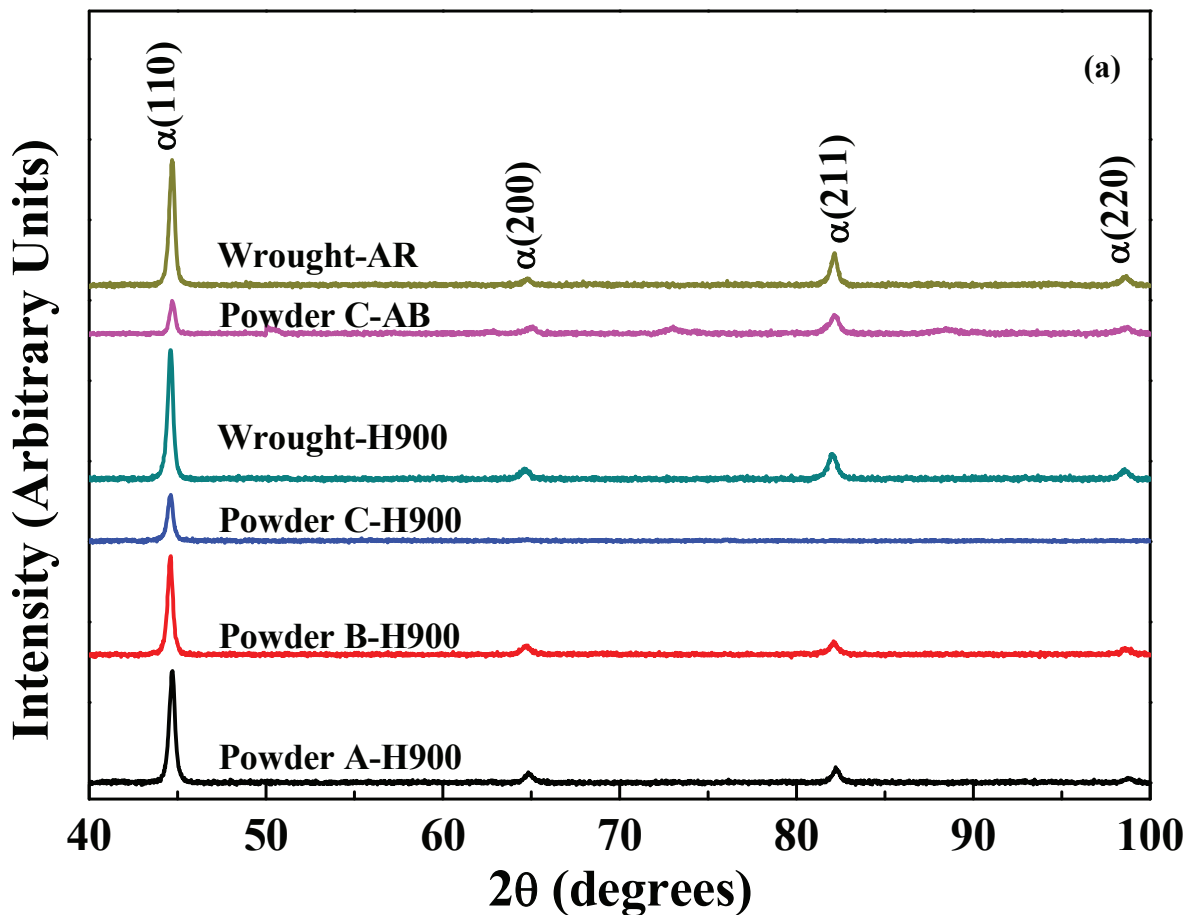


Fig. 5. (100) pole figures along build direction for Powder C-H900 and Wrought H900 samples

Fig. 6(a, b) shows the XRD spectra that were obtained from the specimen sections along the build direction for all three Ar atomized powder and wrought samples. XRD scans from  $40^{\circ}$  to  $50^{\circ}$

diffraction angle with increased step size (2s/step) were obtained to confirm that no low-intensity austenite peak at  $43.5^\circ$  is present. From XRD data no detectable metastable austenite is present in any of these samples. Table 2 details the volume fraction of austenite observed for all the samples from XRD and EBSD analysis. EBSD phase analysis exhibited austenite volume fractions for Powder C-H900 and Wrought-H900 samples are approximately 2.3 and 1.2%, respectively. In general, the standard heat treatment process for 17-4 PH [13, 18, 19] causes austenite reversion from martensite due to the chemical stabilization by the diffusion of the alloying elements. However, XRD and EBSD results indicate that there is no significant austenite reversion occurred in Powder C and wrought samples from H900 heat treatment. All three SLM processed samples have no significant amount of austenite in the as-built condition as well [14]. Out of various possibilities, low concentration of austenite stabilizing elements specifically Ni and Mn in Powder A and Powder B, high cooling rate from SLM fabrication process accompanied by no additional austenite stabilizer such as N<sub>2</sub> gas from powder fabrication process could suppress the austenite transformation from  $\delta$  ferrite upon cooling. More interestingly, EBSD results exhibited lower austenite volume fraction in Powder C-H900 sample compared to the as-built sample indicating that there is no austenite reversion from hardening. XRD patterns also indicate that Powder C-H900 has weaker global texture compared to Wrought-H900 sample by disappearing the BCC ferrite peaks at (200), (211) and (220) along with the reduced relative intensity of (110) peak (Fig. 6(a, b)).



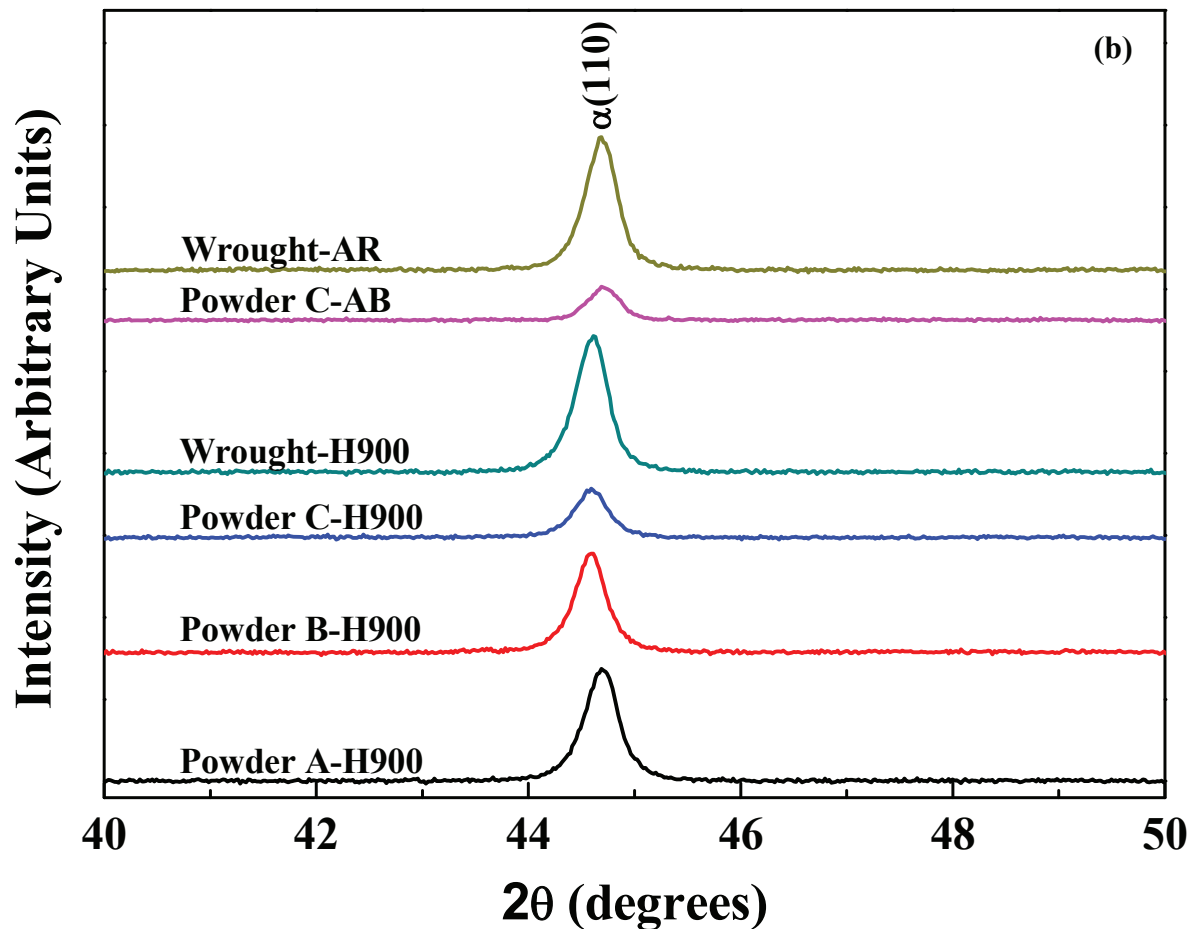


Fig. 6. XRD patterns of all three Ar atomized SLM processed and wrought samples in the as-built/as-received and H900 conditions

**Table 2.** Measured austenite volume fraction from XRD and EBSD

	XRD		EBSD	
	As-built	H900	As-built	H900
Powder A	ND	ND	<1	-
Powder B	~2.6	ND	<1	-
Powder C	ND	ND	~3.7	~2.3
Wrought	ND	ND	-	~1.2

\*- not measured, ND- not detected

## Mechanical Properties

Typical engineering stress-strain curves for SLM and wrought samples in both the as-built and H900 conditions are represented in Fig. 7(a, b). Among the three SLM samples, Powder C-AB sample has higher yield strength with poor elongation and non-uniform plastic deformation in the as-built condition. Overall, the shape of the stress-strain curves for Powder C-AB and Wrought-AR samples are similar that exhibiting a non-uniform plastic deformation from untempered martensitic phase constituent. All the measured mechanical properties are detailed in Table 3. H900 increased the yield strength for all the samples including wrought. Total elongation for all H900 SLM samples weakened after uniform plastic deformation. This observation is consistent with SLM processed 17-4 PH [4]. This could be due to the internal stresses and porosity from the layer-by-layer fabrication of the SLM process. No strain hardening behavior is observed in any of these samples. This can be attributed to the insignificant amount of retained or reverted austenite, which is not sufficient to induce any transformation-induced plasticity (TRIP). Wrought-H900 sample exhibited higher elongation, approximately 17.3%, whereas SLM fabricated sample did not exhibit any improvement in the elongation from H900. The ultimate tensile strength of Powder C-H900 (~1467 MPa) is comparable to Wrought-H900 (~1523 MPa) and is higher than the material standard minimum (~1310 MPa) for H900 followed by a solution heat treatment [20]. Tensile and yield strengths of Powder C-H900 are higher than many reported tensile and yield strengths of SLM processed solutionized and hardened 17-4 PH [4, 13, 21, 22]. Despite lower yield and tensile strengths for Powder A and Powder B samples, the total elongation was observed to be higher in the as-built and H900 conditions compared to Powder C samples. Unlike wrought samples, SLM samples total elongation to failure is not improved with H900 from the as-built condition. However, direct hardening using H900 condition enhanced the uniform elongation for Powder C sample. Vickers microhardness increased with H900 for all the samples (Table 3). Among all SLM processed samples, Powder C-H900 sample exhibited higher microhardness, comparable to Wrought-H900 sample. This result is consistent with the similarity observed in yield and tensile strengths for Powder C-H900 and Wrought-H900 samples. However, tensile results clearly showed the lower total and uniform elongation for Powder C-H900 compared to Wrought-H900 sample.

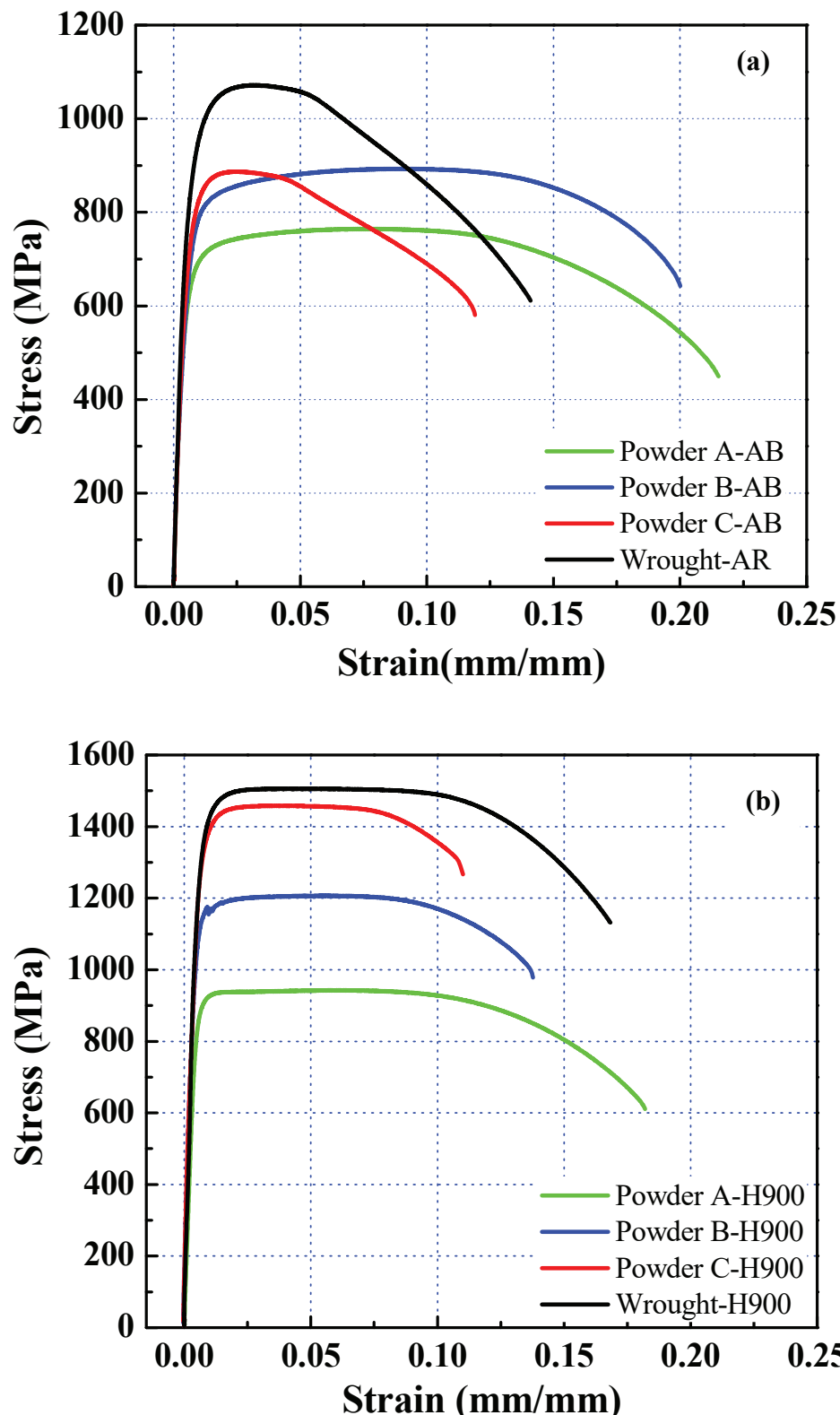


Fig. 7. Representative tensile engineering stress-strain curves for Powder A, Powder B, Powder C and wrought samples (a) as-built, (b) H900

**Table 3.** Summary of mechanical properties showing an average of three measurements

Sample	Yield strength, 0.2% elastic offset (MPa)	Ultimate tensile strength (MPa)	Total elongation (%)	Micro-Vickers hardness (HV)
Powder A-AB	607 ± 14	763 ± 14	22.3 ± 0.7	277.3 ± 10
Powder B-AB	699 ± 17	871 ± 25	19.4 ± 1.0	330.7 ± 9
Powder C-AB	723 ± 13	917 ± 27	10.9 ± 0.9	333.0 ± 5
Powder A-H900	873 ± 7	953 ± 24	16.8 ± 5.4	356.1 ± 10
Powder B-H900	1121 ± 15	1196 ± 20	12.3 ± 2.8	396.3 ± 9
Powder C-H900	1308 ± 30	1467 ± 11	9.3 ± 1.6	461.9 ± 5
Wrought-AR	841 ± 13	1080 ± 13	13.1 ± 1.1	353.9 ± 9
Wrought-H900	1371 ± 52	1523 ± 18	17.3 ± 1.2	480.2 ± 13

### **Conclusions**

In this study, microstructures and mechanical properties of SLM processed 17-4 PH were evaluated with respect to initial powder chemical composition. Mechanical performance varied greatly as a result of the evolution of phases resulting from the disparity in the powder chemical composition and H900 heat treatment. H900 hardening - without prior solutionizing - of SLM sample with low Cr<sub>eq</sub>/Ni<sub>eq</sub> powder resulted in yield and tensile strengths, and microhardness values that are comparable to wrought samples in H900 condition. Wrought total elongation was greater than that for all SLM samples under all conditions. Regardless of the powder chemical composition, no austenite reversion was observed after H900 treatment.

### **Acknowledgments**

The U.S Naval Air Systems Command (NAVAIR) under contract number N68335-18-C-0020 funded the research work reported in this paper. We would like to acknowledge Mitch Gennocro from NAVAIR for serving as the technical mentor for the STTR project. We are grateful to Dr. Keng Hsu and Dr. Anagh Deshpande for their initial support in EBSD characterization.

### **References**

- [1] S. Cheruvathur, E.A. Lass, C.E. Campbell, Additive manufacturing of 17-4 PH stainless steel: post-processing heat treatment to achieve uniform reproducible microstructure, *Jom* 68(3) (2016) 930-942.
- [2] E.A. Lass, M.R. Stoudt, M.E. Williams, Additively Manufactured Nitrogen-Atomized 17-4 PH Stainless Steel with Mechanical Properties Comparable to Wrought, *Metallurgical and Materials Transactions A* 50(4) (2019) 1619-1624.
- [3] A. Yadollahi, N. Shamsaei, S.M. Thompson, A. Elwany, L. Bian, Effects of building orientation and heat treatment on fatigue behavior of selective laser melted 17-4 PH stainless steel, *International Journal of Fatigue* 94 (2017) 218-235.
- [4] M. Mahmoudi, A. Elwany, A. Yadollahi, S.M. Thompson, L. Bian, N. Shamsaei, Mechanical properties and microstructural characterization of selective laser melted 17-4 PH stainless steel, *Rapid Prototyping Journal* 23(2) (2017) 280-294.
- [5] M. Ghayoor, S.B. Badwe, H. Irrinki, S.V. Atre, S. Pasebani, Water Atomized 17-4 PH Stainless Steel Powder as a Cheaper Alternative Powder Feedstock for Selective Laser Melting, *Materials Science Forum* 941 (2019) 698-703.
- [6] L. Carneiro, B. Jalalahmadi, A. Ashtekar, Y. Jiang, Cyclic deformation and fatigue behavior of additively manufactured 17-4 PH stainless steel, *International Journal of Fatigue* 123 (2019) 22-30.
- [7] P.D. Nezhadfar, E. Burford, K. Anderson-Wedge, B. Zhang, S. Shao, S.R. Daniewicz, N. Shamsaei, Fatigue crack growth behavior of additively manufactured 17-4 PH stainless steel: Effects of build orientation and microstructure, *International Journal of Fatigue* 123 (2019) 168-179.
- [8] H.K. Rafi, D. Pal, N. Patil, T.L. Starr, B.E. Stucker, Microstructure and mechanical behavior of 17-4 precipitation hardenable steel processed by selective laser melting, *Journal of materials engineering and performance* 23(12) (2014) 4421-4428.
- [9] Y. Sun, R.J. Hebert, M. Aindow, Effect of heat treatments on microstructural evolution of additively manufactured and wrought 17-4PH stainless steel, *Materials & Design* 156 (2018) 429-440.
- [10] I. Yadroitsev, I. Yadroitsava, Evaluation of residual stress in stainless steel 316L and Ti6Al4V samples produced by selective laser melting, *Virtual and Physical Prototyping* 10(2) (2015) 67-76.
- [11] Y. Liu, Y. Yang, D. Wang, A study on the residual stress during selective laser melting (SLM) of metallic powder, *The International Journal of Advanced Manufacturing Technology* 87(1) (2016) 647-656.
- [12] L.E. Murr, E. Martinez, J. Hernandez, S. Collins, K.N. Amato, S.M. Gaytan, P.W. Shindo, Microstructures and properties of 17-4 PH stainless steel fabricated by selective laser melting, *Journal of Materials Research and Technology* 1(3) (2012) 167-177.
- [13] T. LeBrun, T. Nakamoto, K. Horikawa, H. Kobayashi, Effect of retained austenite on subsequent thermal processing and resultant mechanical properties of selective laser melted 17-4 PH stainless steel, *Materials & Design* 81 (2015) 44-53.
- [14] S. Vunnam, A. Saboo, C. Sudbrack, T.L. Starr, Effect of powder chemical composition on the as-built microstructure of 17-4 PH stainless steel processed by selective laser melting, *Additive Manufacturing* (2019) 100876.
- [15] D. Kotecki, T. Siewert, WRC-1992 constitution diagram for stainless steel weld metals: a modification of the WRC-1988 diagram, *Welding Journal* 71(5) (1992) 171-178.

- [16] S. Dabson, 17-4 PH Stainless Steel Powder Characterization and SLM Part Density, Manuscript under preparation (2019).
- [17] I.L. Dillamore, W.T. Roberts, Rolling textures in f.c.c. and b.c.c. metals, *Acta Metallurgica* 12(3) (1964) 281-293.
- [18] H. Mirzadeh, A. Najafizadeh, Aging kinetics of 17-4 PH stainless steel, *Materials Chemistry and Physics* 116(1) (2009) 119-124.
- [19] U.K. Viswanathan, P.K.K. Nayar, R. Krishnan, Kinetics of precipitation in 17-4 PH stainless steel, *Materials Science and Technology* 5(4) (1989) 346-349.
- [20] ASTM International. ASTM A564/A564M-10 Standard Specification for Hot-Rolled and Cold-Finished Age Hardening Stainless Steel Bars and Shapes.
- [21] A. Yadollahi, N. Shamsaei, S.M. Thompson, A. Elwany, L. Bian, M. Mahmoudi, Fatigue behavior of selective laser melted 17-4 PH stainless steel, 26th International Solid Freeform Fabrication Symposium, Austin, TX, Aug, 2015, pp. 10-12.
- [22] H. Irrinki, S.D. Nath, M. Alhofors, J. Stitzel, O. Gulsoy, S.V. Atre, Microstructures, properties, and applications of laser sintered 17-4PH stainless steel, *Journal of the American Ceramic Society*.